

# Reconfigurable generation of spatial entanglement in nonlinear waveguide arrays

A. Raymond,<sup>1</sup> A. Zecchetto,<sup>1</sup> J. Palomo,<sup>2</sup> M. Morassi,<sup>3</sup> A. Lemaître,<sup>3</sup>  
F. Raineri,<sup>4,3</sup> M.I. Amanti,<sup>1</sup> S. Ducci,<sup>1</sup> and F. Baboux<sup>1,\*</sup>

<sup>1</sup>*Université Paris Cité, CNRS, Laboratoire Matériaux et Phénomènes Quantiques, 75013 Paris, France*

<sup>2</sup>*Laboratoire de Physique de l'École normale supérieure, ENS-PSL,  
Université PSL, CNRS, Sorbonne Université, Paris, France*

<sup>3</sup>*Université Paris-Saclay, CNRS, Centre de Nanosciences et de Nanotechnologies, 91120, Palaiseau, France*

<sup>4</sup>*Université Côte d'Azur, Institut de Physique de Nice, CNRS-UMR 7010, Nice 06200, France*

(Dated: May 15, 2024)

Harnessing high-dimensional entangled states of light presents a frontier for advancing quantum information technologies, from fundamental tests of quantum mechanics to enhanced computation and communication protocols. In this context, the spatial degree of freedom stands out as particularly suited for on-chip integration. But while traditional demonstrations produce and manipulate path-entangled states sequentially with discrete optical elements, continuously-coupled nonlinear waveguide systems offer a promising alternative where photons can be generated and interfere along the entire propagation length, unveiling novel capabilities within a reduced footprint. Here we exploit this concept to implement a compact and reconfigurable source of spatially entangled photon pairs based on parametric down-conversion in AlGaAs nonlinear waveguide arrays. We use a double-pump configuration to engineer the output quantum state and implement various types of spatial correlations, exploiting a quantum interference effect between the biphoton state generated in each pumped waveguide. This demonstration, at room temperature and telecom wavelength, illustrates the potential of continuously-coupled systems as a promising alternative to discrete multi-component quantum circuits for leveraging the high-dimensional spatial degree of freedom of photons.

Nonclassical states of light constitute crucial resources for quantum information technologies due to their ability to transmit easily, resist decoherence, and offer various ways to encode information [1]. Recently, considerable attention has been devoted to entanglement in high-dimensional degrees of freedom of photons [2] to push fundamental tests of quantum mechanics [3, 4], boost the efficiency and security of quantum communication [5, 6], and make quantum computing more flexible [7, 8].

Among the various candidates, the spatial degree of freedom emerges as especially fitted for on-chip integration [9, 10]. Rapid progress has thus been made in recent years to develop complex integrated circuits achieving on-chip quantum interference [11], entanglement and various logical operations on spatially encoded states [12, 13], in the spirit of the gate-based model of quantum information processing [14]. These powerful demonstrations typically implement a discrete and sequential manipulation of path-entangled states using beamplitters and phase shifters, with most of the footprint devoted to routing waveguides.

Another route to spatial entanglement is however possible, based on continuously-coupled waveguides [15, 16] where photons can interfere across the entire propagation length rather than solely at individual beamplitters. This approach implements continuous-time random quantum walks [17] and can be described by a lattice Hamiltonian [15], establishing a natural connection with a variety of situations encountered in condensed matter physics. Arrays of coupled waveguides have recently facilitated investigations into a large spectrum of phe-

nomena spanning quantum walks of correlated photons [18–20], Anderson localization of photon pairs [21], quantum logic operations [22, 23], topological effects [24, 25] or synthetic dimensions [26]. These remarkable achievements have relied on external sources to generate quantum states of light, which were then fed into a passive circuitry.

Yet, an additional layer of complexity can introduce even larger possibilities, by adding to the continuous nature of the interference process the ability to continuously generate photons all along the device. This can be realized in a waveguide array made out of a nonlinear material, by injecting a classical pump beam generating stochastically photon pairs by spontaneous parametric down-conversion (SPDC) or four-wave mixing [27–30]. This approach offers novel configurations that have no equivalent in bulk optics nor discrete photonic circuits due to the intricate combination of the generation and manipulation steps of photonic quantum states [31–33].

In this work, we exploit this concept in AlGaAs-based nonlinear waveguide arrays to implement a compact and versatile source of spatially entangled states of light, operating at room temperature and telecom wavelength. We use a double-pump configuration to engineer the output quantum state and implement different types of spatial correlations, violating a non-classicality criterion by several tens of standard deviations. This control relies on a quantum interference effect between the biphoton wavefunction generated in each pumped waveguide, which is fully accounted for by analytical calculations and numerical simulations. Coupled with the high integration capabilities of the AlGaAs platform [34, 35] and the ability to implement diverse lattice geometries, this demonstration paves the way to quantum information

---

\* Corresponding author: florent.baboux@u-paris.fr

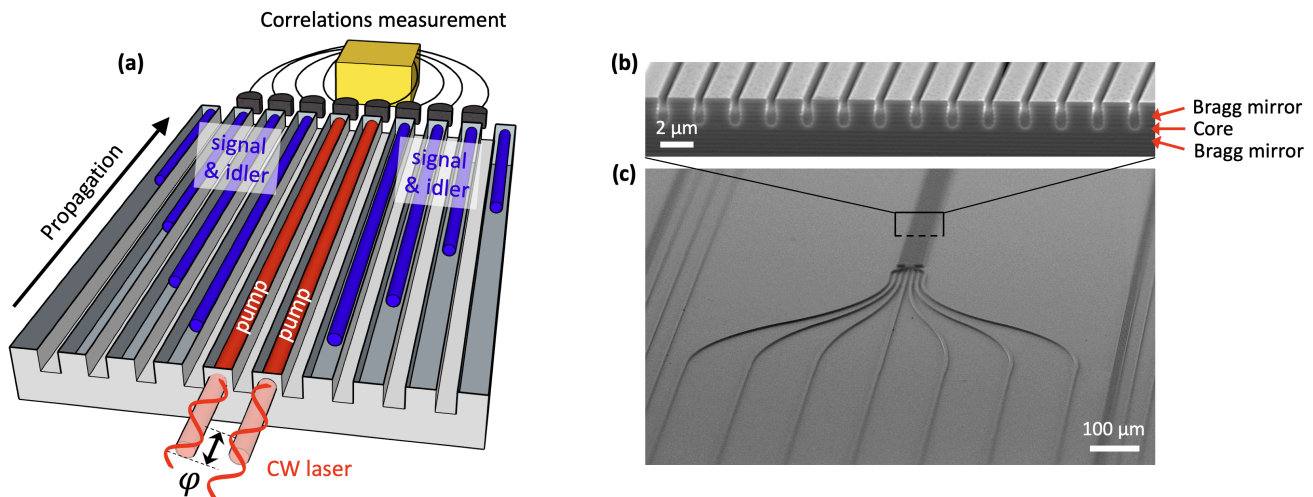


FIG. 1. (a) Principle of the spatial entanglement engineering in an AlGaAs nonlinear waveguide array. Here, two continuous-wave pump laser beams (sketched in red) with a phase offset  $\varphi$  between them generate photon pairs that undergo quantum walks (blue), resulting in spatial entanglement over the whole lattice. (b) SEM image of a fabricated sample, showing a cut of the waveguide array in the central part. (c) Wider-field SEM image showing the array connected to S-bend waveguides for the individual optical addressing of each spatial channel.

tasks leveraging the high-dimensional spatial degree of freedom in continuously-coupled photonic systems.

The working principle of our AlGaAs nonlinear waveguide array is sketched in Fig. 1a. A classical pump beam (wavelength  $\simeq 775$  nm, sketched in red) injected into one or several waveguides generates photon pairs at telecom wavelength ( $\simeq 1550$  nm, shown in blue) by SPDC, thanks to the strong  $\chi^{(2)}$  nonlinearity of the material. These photon pairs can continuously tunnel from one waveguide to the other during their propagation, implementing random quantum walks. Compared to quantum walks in passive circuits [18–20], the walkers are here generated directly inside the device and the generation can take place at any position along the propagation axis. Besides a gain of integration, this configuration allows for a significantly higher level of spatial entanglement, due to the interference between quantum walks initiated at all possible longitudinal positions [27]. The device is designed so that the transverse coupling of the pump beam is negligible (which is naturally favored by its twice shorter wavelength), so that the pump remains confined in the initially pumped waveguide(s) during propagation.

The evanescent coupling of the telecom (SPDC) modes in the array introduces a discretized dispersion relation (band structure), modifying the propagation constant in the longitudinal direction. For a given mode polarization, it reads

$$\beta(\omega, k) = \beta^{(0)}(\omega) + 2C(\omega) \cos(k) \quad (1)$$

where  $\beta^{(0)}(\omega) = \omega n_{\text{eff}}(\omega)/c$  is the propagation constant of a single waveguide at frequency  $\omega$ , governed by the effective refractive index  $n_{\text{eff}}(\omega)$ . The second term, where  $C$  is the evanescent coupling constant and  $k$  is the dimensionless transverse wavevector (normalized to  $1/a$ , where  $a$  is the lattice periodicity), which defines the phase difference between the neighboring waveguides,

corresponds to the modification of the dispersion relation induced by the presence of the array. For a given  $\omega$ , Eq. (1) is analogous to the dispersion relation of an electron in a periodic potential, as obtained in the tight-binding approximation, and the  $\beta(\omega, k)$  correspond to the Bloch modes of the lattice.

After SPDC generation in the array under a monochromatic pump beam (frequency  $\omega_p$ ), and filtering the signal and idler around degeneracy (i.e. with frequencies  $\omega_s \simeq \omega_i \simeq \omega_p/2$ ), the biphoton state at the output can be written as a superposition of spatial modes, governed by the complex-valued function

$$\phi_k(k_s, k_i) = \tilde{A}_p(k_s + k_i) \text{sinc}(\Delta\beta(k_s, k_i) L/2) e^{i\Delta\beta(k_s, k_i) \frac{L}{2}} \quad (2)$$

which determines the probability to generate, from an input pump photon, a photon pair with the signal and idler in Bloch modes  $k_s$  and  $k_i$  respectively [36]. In this expression,  $\tilde{A}_p$  is the spatial Fourier transform of the pump field (determined by its amplitude in each waveguide, and written here by taking into account the conservation of the transverse wavevector), and  $L$  is the longitudinal length of the array. In order to obtain a significant pair generation rate, the phase-matching condition  $\Delta\beta = 0$  must be nearly perfectly satisfied, with  $\Delta\beta$  given by

$$\Delta\beta(k_s, k_i) = \Delta\beta^{(0)} - 2C_s \cos(k_s) - 2C_i \cos(k_i) \quad (3)$$

Here,  $\Delta\beta^{(0)}$  is the phase-mismatch of a single (uncoupled) waveguide, which depends on the pump frequency, and  $C_s = C_s(\omega_p/2)$  and  $C_i = C_i(\omega_p/2)$  are the coupling constants of the signal and idler photons in their corresponding polarization. For a given pump frequency, the spatial correlations can thus be controlled by tailoring the spatial profile of the pump beam (term  $\tilde{A}_p$  in Eq. (2)), providing the principle for a compact and reconfigurable source of spatially entangled states of

light. The spatial correlations in real space are described by a (symmetric) matrix  $\Gamma_{n_s, n_i} = |\phi_n(n_s, n_i)|^2$ , where  $\phi_n(n_s, n_i)$  is the Fourier transform of  $\phi_k$ . Note that  $\Gamma_{n_s, n_i}$  is not normalized to unity, it takes into account the SPDC efficiency and hence is directly proportional to coincidence counts as will be measured experimentally in the following.

The investigated sample consists in an array of 31 coupled AlGaAs waveguides of length  $L = 2$  mm (Fig. 1b). The waveguides are 1.7  $\mu\text{m}$ -wide and separated by 450 nm gaps. The 7 central waveguides of the array are connected to fan-in injection waveguides and fan-out collection waveguides to facilitate their individual optical addressing (Fig. 1c). These injection and collection waveguides have a larger width (6  $\mu\text{m}$ ) to shift their nonlinear resonance wavelength (by 10 nm), so that the injected pump laser generates photon pairs only in the central array region. The total longitudinal length of the sample is 4.3 mm.

The epitaxial structure is made of a stacking of AlGaAs layers with alternating Aluminum concentrations. On each side of the waveguides core, two Bragg mirrors provide both a photonic band-gap confinement for the pump beam in the NIR range (at  $\simeq 775$  nm) and total internal reflection claddings for the produced SPDC photons in the telecom range ( $\simeq 1550$  nm). Therefore, the pump and SPDC modes are characterized by different dispersion curves, allowing the single-waveguide phase-matching condition  $\Delta\beta^{(0)} = 0$  to be satisfied in the spectral range of interest [35, 37–39]. The epitaxial structure is grown by molecular beam epitaxy, and the sample is processed by electron-beam lithography (using a high-resolution HSQ resist) followed by ICP dry etching. The determined propagation losses are of 0.6  $\text{cm}^{-1}$  at telecom wavelength.

The experiments are carried out by injecting a TE-polarized continuous-wave pump laser with a microscope objective into one or several waveguides (depending on the targeted quantum state), to generate by orthogonally polarized signal and idler photons by type-2 SPDC in the array region. These SPDC photons undergo random quantum walks and are collected at the output of the fan-out waveguides using a commercial lensed fiber array connected to superconducting nanowire single-photon detectors (SNSPD). Correlation events are measured by a time tagger: coincidences between distinct waveguides (i.e. off-diagonal points in the spatial correlation matrix  $\Gamma_{n_s, n_i}$ ) are determined directly using this setup, while coincidences within each waveguide (diagonal correlations) are determined using an additional beamsplitter after each waveguide to split the SPDC photons into its two outputs (with 50% probability) before detection.

The pump laser is first injected into the central waveguide ( $n = 0$ ) of the array, and coincidences are monitored as a function of the laser wavelength for a coupled pump power of  $\simeq 1$  mW. Here and in the subsequent measurements, a bandpass filter is used before photon detection to reduce the emission bandwidth to 16 nm and effectively suppress (up to 1%) any possible coupling be-

tween the spatial and spectral properties of the biphoton states [36]. As shown in Fig. 2a, the coincidences in the central waveguide ( $\Gamma_{0,0}$ , black points) show a resonance centered at  $\lambda_{p,0} = 783.45$  nm, which corresponds (up to 0.05 nm) to the resonance wavelength which we measured for a single (uncoupled) waveguide, i.e. the pump wavelength that satisfies  $\Delta\beta^{(0)} = 0$ . The diagonal coincidences ( $\Gamma_{1,1} + \Gamma_{-1,-1}$ , red points) and antidiagonal coincidences ( $\Gamma_{1,-1} + \Gamma_{-1,1}$ , blue points) display a similar resonant behavior.

We next set the pump wavelength to  $\lambda_{p,0}$  and proceed to the measurement of the full correlation matrix within the Hilbert space formed by the 5 central waveguides. The result is shown in Fig. 2b and compared to numerical simulations in Fig. 2f. As anticipated by the results of Fig. 2a, we observe strong and selective correlations along the diagonal and the antidiagonal axes. That is, photons have an enhanced probability to exit the device either through the same waveguide ( $n_s = n_i$ , spatial bunching) or through opposite waveguides ( $n_s = -n_i$ , spatial antibunching). Indeed, since  $\Delta\beta^{(0)} = 0$  the phase-matching condition  $\Delta\beta \simeq 0$  selects the Bloch modes satisfying  $\cos(k_s) + \cos(k_i) \simeq 0$ , corresponding to  $k_s \pm k_i \simeq \pm\pi$  [36]. This corresponds to equal or opposite transverse propagation velocities for the twin photons,  $v(k_s) = \pm v(k_i)$ , giving rise to both a bunching and antibunching pattern [27].

The non-classicality of the measured correlations can be quantified by using the criteria derived by Bromberg et al. [16, 18]. For classical light, the diagonal and off-diagonal correlations must satisfy the inequality  $\Gamma_{n_i, n_s} \geq \frac{1}{3} \sqrt{\Gamma_{n_i, n_i} \Gamma_{n_s, n_s}}$ . For the measured state of Fig. 2b, this inequality is violated (up to 10 standard deviations) by several points of the measured correlation matrix [36], indicating spatial correlations that cannot be generated by classical means. From the total detected coincidences counts and the measured collection and detection efficiency, the generation rate of these quantum states at the chip output is  $1.2 \times 10^5$  Hz/mW of internal pump power, within a nonlinear generation length of 2 mm. The overlap between the experimental ( $\Gamma_{n_s, n_i}^{\text{exp}}$ ) and theoretical ( $\Gamma_{n_s, n_i}^{\text{th}}$ ) correlations matrices can be quantified using the similarity parameter [18, 19]  $S = (\sum \sqrt{\Gamma_{n_s, n_i}^{\text{exp}} \Gamma_{n_s, n_i}^{\text{th}}})^2 / (\sum \Gamma_{n_s, n_i}^{\text{exp}} \sum \Gamma_{n_s, n_i}^{\text{th}})$ . We obtain  $S = 98.4 \pm 1.1\%$  (without adjustable parameter), illustrating the high fidelity of the source.

We will now show how this map of spatial correlations can be flexibly engineered by tailoring the pumping configuration. For this we coherently pump two neighboring waveguides ( $n = 0$  and 1) by splitting the CW pump laser into a bulk interferometer placed before the injection objective, allowing to inject two laser beams of equal intensity (0.5 mW) and controlled phase  $\varphi$  between them (see Fig. 1a). The effect of this phase offset is first investigated by monitoring the crossed coincidences  $\Gamma_{0,1}$  between the two pumped waveguides as a function of  $\varphi$ , as shown in Fig. 2e (green circles). An oscillating behavior is observed, well reproduced by a sinusoidal modulation (black line) with a net (raw) visibility of 90% (85%).



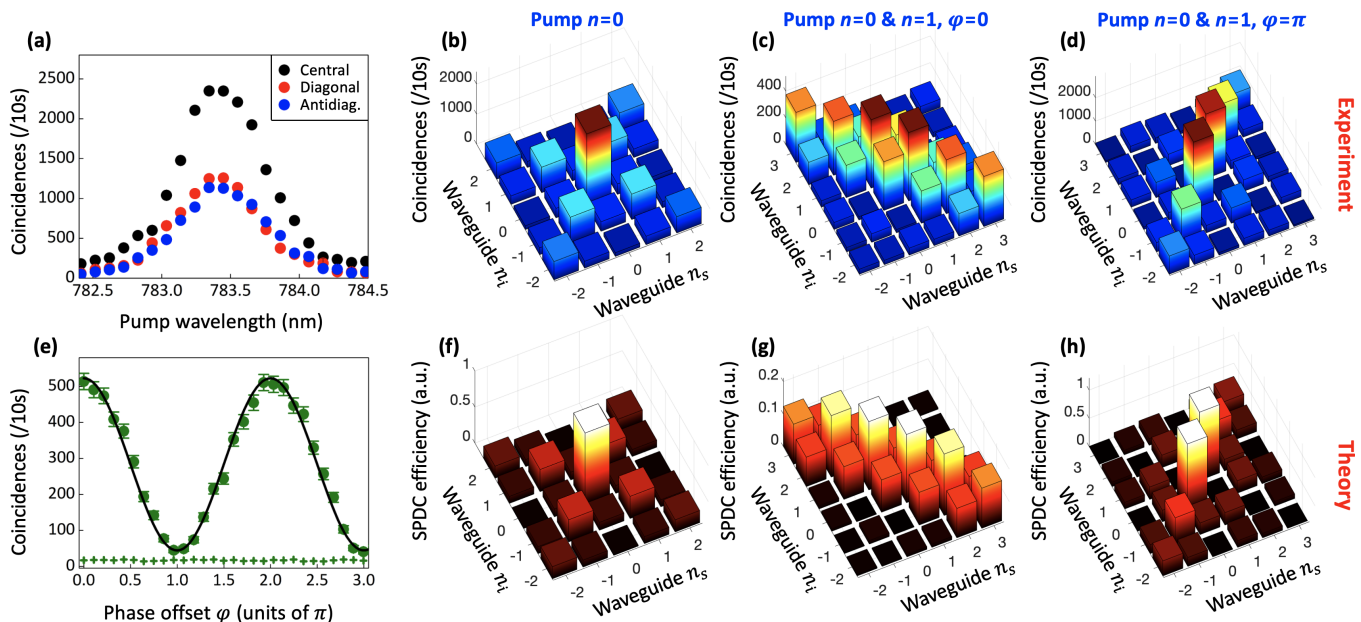


FIG. 2. (a) Biphoton correlations measured in the central waveguide ( $\Gamma_{0,0}$ , black), first diagonal ( $\Gamma_{1,1} + \Gamma_{-1,-1}$ , red) and first anti-diagonal ( $\Gamma_{1,-1} + \Gamma_{-1,1}$ , blue) points of the correlation matrix when pumping the  $n = 0$  waveguide (raw coincidence counts). (b-c-d) Measured correlation matrices when pumping (b) the central waveguide  $n = 0$ , (c) guides  $n = 0$  and  $n = 1$  in phase and (d) guides  $n = 0$  and  $n = 1$  out of phase. (e) Cross-correlation term  $\Gamma_{0,1}$  measured for varying phase offset  $\varphi$  between the two pumped waveguides ( $n = 0$  and  $1$ ); circles show raw coincidence counts with Poissonian error bar, crosses show noise counts, and the black line is a sinusoidal fit. (f-g-h) Numerically simulated correlation matrices corresponding to the experimental cases (b-c-d); the efficiency unit is the same for all three panels and can thus be directly compared to the experiment.

This behavior is in good qualitative agreement with our analytical calculations which predict (in the limit of an infinite lattice and perfect spectral degeneracy):

$$\Gamma_{0,1} \propto (1 + \cos \varphi), \quad (4)$$

corresponding to an alternation of (full) destructive and constructive interference of the biphoton wavefunction at this point of the correlation matrix [36].

We now set  $\varphi = 0$  and measure the spatial correlation matrix within the 6-waveguide basis centered on the pumped waveguides. The result is shown in Fig. 2c and compared to numerical simulations in Fig. 2g (similarity  $93.1 \pm 1.8\%$ ). We observe this time strong correlations along the anti-diagonal, showing that spatial antibunching is selectively enhanced by this pumping configuration. We also notice, compared to the single-pump case (Fig. 2b), a wider propagation of the biphoton correlations, which decrease only slowly over the 6 measured waveguides.

We then set  $\varphi = \pi$ , corresponding to the  $n = 0$  and  $n = 1$  waveguides pumped in phase opposition. The measured correlation matrix is shown in Fig. 2d along with simulation results in 2h (similarity  $96.9 \pm 1.0\%$ ). In this case, we observe that spatial bunching is selectively enhanced, while the spreading of correlations is comparable to the single-pump configuration. However, the total SPDC signal (integrated over all measured points of the correlation matrix) is stronger (by a factor  $\simeq 2.8$ ) for  $\varphi = \pi$  than for  $\varphi = 0$ , despite the fact that the input

pump power is the same. As the transverse coupling of the pump beam is negligible, the two pump beams do not interfere classically and this interference effect is of quantum nature: the biphoton states generated in the two pumped waveguides interfere constructively when  $\varphi = \pi$  and destructively when  $\varphi = 0$ , and it can be shown analytically [36] that the total SPDC intensity is modulated as

$$\sum_{n_s, n_i} \Gamma_{n_s, n_i} \propto (2 - \cos \varphi) \quad (5)$$

when the phase  $\varphi$  between the two pumped waveguides is varied.

This intriguing behavior, with a constructive interference occurring for out-of-phase pumping, can be understood intuitively in the following manner. In the single-pump configuration, correlations are mainly located on the diagonal and anti-diagonal (Figs. 2b,f). According to coupled-mode theory, a single photon acquires a phase of  $\pi/2$  when it tunnels to a neighboring waveguide; hence, starting from its generation in the central waveguide  $n = 0$ , the biphoton state acquires a phase  $\pi$  when it moves one step along the diagonal or the anti-diagonal, as this requires two single-photon jumps (either on the same or on opposite sides). The phase of the wavefunction thus changes by  $\pi$  between each two successive points along the diagonal and anti-diagonal. Now, when pumping two neighboring waveguides  $n = 0$  and  $1$ , an interference occurs between the biphoton states  $|\Psi\rangle_{n=0}$

and  $|\Psi\rangle_{n=1}$  generated in these two waveguides. When the two pumps are in phase (resp. out of phase), this interference is destructive (resp. constructive) on the diagonal points (which are aligned for the two states) because of the  $\pi$  phase alternation structure described above, in good agreement with the experiments and simulations. This interference is only partial since the two biphoton states have different amplitudes on the interfering points; however it plays a determinant role in the total SPDC efficiency since an important part of the signal is concentrated in each pumped waveguide, providing an intuitive argument for the total SPDC intensity being maximum when  $\varphi = \pi$ , in agreement with Eq. (5). The situation is reversed in the case of antidiagonal points. However, on the antidiagonal passing through  $(0, 1)$  the two biphoton states interfere with the exact same amplitude, leading to a perfect interference and thus a high spatial spreading of the correlations when  $\varphi = 0$ , in good agreement with Figs. 2c and 2g. This demonstrated quantum interference effect provides the building block for engineering spatially entangled states in continuously-coupled nonlinear waveguides.

In summary, we have demonstrated a compact and versatile source of spatial entanglement based on quantum walks in semiconductor AlGaAs nonlinear waveguide arrays. Tailoring the spatial profile of the pump field allows to reconfigure the output quantum state and implement various types of spatial correlations, well accounted for by analytical calculations and numerical simulations. Building upon these results, a wider zoology of quantum states could be produced by pumping more waveguides, with controlled intensity and phase relation between them. To achieve this in an efficient and scalable manner, on-chip beamsplitters and phase shifters based on the strong electro-optic effect of AlGaAs [35, 40] could be integrated prior the generation stage. Pushing further the integration, the possibility to integrate the pump laser directly within the nonlinear medium [39], to ob-

tain a fully standalone source, constitutes a distinctive asset of the AlGaAs platform compared to dielectric and silicon-based photonic circuits where spatially entangled states have been studied previously [9].

In addition, the strong second-order nonlinearity of AlGaAs could be leveraged to push nonlinear waveguide arrays into the squeezing regime [41, 42]. In line with recent theoretical studies, this approach is expected to enable the generation of highly multimode squeezed states in a flexible manner [31–33], establishing promising connections with other continuous-variable multimode platforms such as optical frequency combs [43]. Finally, other lattice geometries can be envisaged to investigate various types of physical phenomena: e.g. modulating the coupling distances according to a Fibonacci [44] or Harper [24] sequence would allow investigating topological protection in the quantum regime, while introducing disorder would enable studying the Anderson localization of multi-particle states. Combined with the possibility of engineering losses to investigate non-Hermitian effects [45] or dynamically modulating the array to harness synthetic dimensions [46, 47], these perspectives make the demonstrated platform appealing to simulate in a controlled environment physical problems otherwise difficult to access in condensed-matter systems.

## ACKNOWLEDGMENTS

We thank P. Milman, L. Guidoni and I. Carusotto for fruitful discussion and P. Filloux for technical support. We acknowledge support from the Ville de Paris Emergence program (LATTICE project), Region Ile de France in the framework of the DIM QuantiP (Q-LAT project), IdEx Université de Paris (ANR-18-IDEX-0001), and the French RENATECH network.

- 
- [1] I. Walmsley, Quantum optics: Science and technology in a new light, *Science* **348**, 525 (2015).
  - [2] M. Erhard, M. Krenn, and A. Zeilinger, Advances in high-dimensional quantum entanglement, *Nature Reviews Physics* **2**, 365 (2020).
  - [3] A. C. Dada, J. Leach, G. S. Buller, M. J. Padgett, and E. Andersson, Experimental high-dimensional two-photon entanglement and violations of generalized Bell inequalities, *Nature Physics* **7**, 677 (2011).
  - [4] X.-D. Yu, I. Veeren, and O. Gühne, Characterizing high-dimensional quantum contextuality, *Phys. Rev. A* **109**, L030201 (2024).
  - [5] Y. Ding, D. Bacco, K. Dalgaard, X. Cai, X. Zhou, K. Rottwitz, and L. K. Oxenløwe, High-dimensional quantum key distribution based on multicore fiber using silicon photonic integrated circuits, *npj Quantum Information* **3**, 25 (2017).
  - [6] D. Cozzolino, B. Da Lio, D. Bacco, and L. K. Oxenløwe, High-dimensional quantum communication: benefits, progress, and future challenges, *Advanced Quantum Technologies* **2**, 1900038 (2019).
  - [7] C. Reimer, S. Sciara, P. Roztock, M. Islam, L. R. Cortés, Y. Zhang, B. Fischer, S. Loranger, R. Kashyap, A. Cino, *et al.*, High-dimensional one-way quantum processing implemented on d-level cluster states, *Nature Physics* **15**, 148 (2019).
  - [8] S. Paesani, J. F. F. Bulmer, A. E. Jones, R. Santagati, and A. Laing, Scheme for universal high-dimensional quantum computation with linear optics, *Phys. Rev. Lett.* **126**, 230504 (2021).
  - [9] A. S. Solntsev and A. A. Sukhorukov, Path-entangled photon sources on nonlinear chips, *Reviews in Physics* **2**, 19 (2017).
  - [10] J. Wang, F. Sciarrino, A. Laing, and M. G. Thompson, Integrated photonic quantum technologies, *Nature Photonics* **14**, 273 (2020).
  - [11] A. Politi, M. J. Cryan, J. G. Rarity, S. Yu, and J. L. O’Brien, Silica-on-silicon waveguide quantum circuits,

- Science **320**, 646 (2008).
- [12] J. Carolan, C. Harrold, C. Sparrow, E. Martín-López, N. J. Russell, J. W. Silverstone, P. J. Shadbolt, N. Matsuda, M. Oguma, M. Itoh, *et al.*, Universal linear optics, Science **349**, 711 (2015).
- [13] J. Wang, S. Paesani, Y. Ding, R. Santagati, P. Skrzypczyk, A. Salavrakos, J. Tura, R. Augusiak, L. Mančinska, D. Bacco, *et al.*, Multidimensional quantum entanglement with large-scale integrated optics, Science **360**, 285 (2018).
- [14] E. Knill, R. Laflamme, and G. J. Milburn, A scheme for efficient quantum computation with linear optics, Nature **409**, 46 (2001).
- [15] H. B. Perets, Y. Lahini, F. Pozzi, M. Sorel, R. Morandotti, and Y. Silberberg, Realization of quantum walks with negligible decoherence in waveguide lattices, Phys. Rev. Lett. **100**, 170506 (2008).
- [16] Y. Bromberg, Y. Lahini, R. Morandotti, and Y. Silberberg, Quantum and classical correlations in waveguide lattices, Phys. Rev. Lett. **102**, 253904 (2009).
- [17] E. Farhi and S. Gutmann, Quantum computation and decision trees, Phys. Rev. A **58**, 915 (1998).
- [18] A. Peruzzo, M. Lobino, J. C. Matthews, N. Matsuda, A. Politi, K. Poulios, X.-Q. Zhou, Y. Lahini, N. Ismail, K. Wörhoff, *et al.*, Quantum walks of correlated photons, Science **329**, 1500 (2010).
- [19] Z.-Q. Jiao, J. Gao, W.-H. Zhou, X.-W. Wang, R.-J. Ren, X.-Y. Xu, L.-F. Qiao, Y. Wang, and X.-M. Jin, Two-dimensional quantum walks of correlated photons, Optica **8**, 1129 (2021).
- [20] F. Hoch, S. Piacentini, T. Giordani, Z.-N. Tian, M. Iuliano, C. Esposito, A. Camillini, G. Carvacho, F. Ceccarelli, N. Spagnolo, *et al.*, Reconfigurable continuously-coupled 3D photonic circuit for boson sampling experiments, npj Quantum Information **8**, 55 (2022).
- [21] G. Di Giuseppe, L. Martin, A. Perez-Leija, R. Keil, F. Dreisow, S. Nolte, A. Szameit, A. F. Abouraddy, D. N. Christodoulides, and B. E. A. Saleh, Einstein-Podolsky-Rosen spatial entanglement in ordered and Anderson photonic lattices, Phys. Rev. Lett. **110**, 150503 (2013).
- [22] Y. Lahini, G. R. Steinbrecher, A. D. Bookatz, and D. Englund, Quantum logic using correlated one-dimensional quantum walks, npj Quantum Information **4**, 2 (2018).
- [23] R. J. Chapman, S. Häusler, G. Finco, F. Kaufmann, and R. Grange, Quantum logical controlled-not gate in a lithium niobate-on-insulator photonic quantum walk, Quantum Science and Technology **9**, 015016 (2023).
- [24] J.-L. Tambasco, G. Corrielli, R. J. Chapman, A. Crespi, O. Zilberberg, R. Osellame, and A. Peruzzo, Quantum interference of topological states of light, Science Advances **4**, eaat3187 (2018).
- [25] F. Klauck, M. Heinrich, and A. Szameit, Photonic two-particle quantum walks in Su–Schrieffer–Heeger lattices, Photonics Research **9**, A1 (2021).
- [26] L. J. Maczewsky, K. Wang, A. A. Dovgiy, A. E. Miroshnichenko, A. Moroz, M. Ehrhardt, M. Heinrich, D. N. Christodoulides, A. Szameit, and A. A. Sukhorukov, Synthesizing multi-dimensional excitation dynamics and localization transition in one-dimensional lattices, Nature Photonics **14**, 76 (2020).
- [27] A. S. Solntsev, A. A. Sukhorukov, D. N. Neshev, and Y. S. Kivshar, Spontaneous parametric down-conversion and quantum walks in arrays of quadratic nonlinear waveguides, Phys. Rev. Lett. **108**, 023601 (2012).
- [28] R. Kruse, F. Katzschnmann, A. Christ, A. Schreiber, S. Wilhelm, K. Laiho, A. Gábris, C. S. Hamilton, I. Jex, and C. Silberhorn, Spatio-spectral characteristics of parametric down-conversion in waveguide arrays, New Journal of Physics **15**, 083046 (2013).
- [29] A. S. Solntsev, F. Setzpfandt, A. S. Clark, C. W. Wu, M. J. Collins, C. Xiong, A. Schreiber, F. Katzschnmann, F. Eilenberger, R. Schiek, W. Sohler, A. Mitchell, C. Silberhorn, B. J. Eggleton, T. Pertsch, A. A. Sukhorukov, D. N. Neshev, and Y. S. Kivshar, Generation of nonclassical biphoton states through cascaded quantum walks on a nonlinear chip, Phys. Rev. X **4**, 031007 (2014).
- [30] A. Blanco-Redondo, B. Bell, D. Oren, B. J. Eggleton, and M. Segev, Topological protection of biphoton states, Science **362**, 568 (2018).
- [31] D. Barral, N. Belabas, L. M. Procopio, V. D’Auria, S. Tanzilli, K. Bencheikh, and J. A. Levenson, Continuous-variable entanglement of two bright coherent states that never interacted, Phys. Rev. A **96**, 053822 (2017).
- [32] D. Barral, M. Walschaers, K. Bencheikh, V. Parigi, J. A. Levenson, N. Treps, and N. Belabas, Quantum state engineering in arrays of nonlinear waveguides, Physical Review A **102**, 043706 (2020).
- [33] D. Barral, K. Bencheikh, J. A. Levenson, and N. Belabas, Scalable multimode entanglement based on efficient squeezing of propagation eigenmodes, Phys. Rev. Res. **3**, 013068 (2021).
- [34] C. P. Dietrich, A. Fiore, M. G. Thompson, M. Kamp, and S. Höfling, GaAs integrated quantum photonics: Towards compact and multi-functional quantum photonic integrated circuits, Laser & Photonics Reviews **10**, 870 (2016).
- [35] F. Baboux, G. Moody, and S. Ducci, Nonlinear integrated quantum photonics with AlGaAs, Optica **10**, 917 (2023).
- [36] See Supplemental Material for additional details on the experiment and the theoretical analysis.
- [37] A. S. Helmy, P. Abolghasem, J. Stewart Aitchison, B. J. Bijlani, J. Han, B. M. Holmes, D. C. Hutchings, U. Younis, and S. J. Wagner, Recent advances in phase matching of second-order nonlinearities in monolithic semiconductor waveguides, Laser & Photonics Reviews **5**, 272 (2011).
- [38] R. Horn, P. Abolghasem, B. J. Bijlani, D. Kang, A. Helmy, and G. Weihs, Monolithic source of photon pairs, Phys. Rev. Lett. **108**, 153605 (2012).
- [39] F. Boitier, A. Orioux, C. Autebert, A. Lemaître, E. Galopin, C. Manquest, C. Sirtori, I. Favero, G. Leo, and S. Ducci, Electrically injected photon-pair source at room temperature, Phys. Rev. Lett. **112**, 183901 (2014).
- [40] J. Wang, A. Santamato, P. Jiang, D. Bonneau, E. Engin, J. W. Silverstone, M. Lermer, J. Beetz, M. Kamp, S. Höfling, *et al.*, Gallium arsenide quantum photonic waveguide circuits, Optics Communications **327**, 49 (2014).
- [41] A. Brodutch, R. Marchildon, and A. S. Helmy, Dynamically reconfigurable sources for arbitrary Gaussian states in integrated photonics circuits, Optics Express **26**, 17635 (2018).
- [42] Z. Yan, H. He, H. Liu, M. Iu, O. Ahmed, E. Chen, P. Blakey, Y. Akasaka, T. Ikeuchi, and A. S. Helmy,  $\chi^{(2)}$ -based AlGaAs phase sensitive amplifier with record gain, noise, and sensitivity, Optica **9**, 56 (2022).

- [43] Y. Cai, J. Roslund, G. Ferrini, F. Arzani, X. Xu, C. Fabre, and N. Treps, Multimode entanglement in reconfigurable graph states using optical frequency combs, *Nature communications* **8**, 15645 (2017).
- [44] F. Baboux, E. Levy, A. Lemaître, C. Gómez, E. Galopin, L. Le Gratiet, I. Sagnes, A. Amo, J. Bloch, and E. Akkermans, Measuring topological invariants from generalized edge states in polaritonic quasicrystals, *Phys. Rev. B Rapid Comm.* **95**, 161114 (2017).
- [45] W. Song, W. Sun, C. Chen, Q. Song, S. Xiao, S. Zhu, and T. Li, Breakup and recovery of topological zero modes in finite non-hermitian optical lattices, *Phys. Rev. Lett.* **123**, 165701 (2019).
- [46] L. Yuan, Q. Lin, M. Xiao, and S. Fan, Synthetic dimension in photonics, *Optica* **5**, 1396 (2018).
- [47] F. S. Piccioli, A. Szameit, and I. Carusotto, Topologically protected frequency control of broadband signals in dynamically modulated waveguide arrays, *Physical Review A* **105**, 053519 (2022).